

Plasma Sci. Technol. **27** (2025) 035504 (10pp)
https://cstr.cn/32219.14.2058-6272/ada21e
https://doi.org/10.1088/2058-6272/ada21e

Preliminary study on degradation mechanisms of plasma-treated DR1 by atomistic simulations

Namunakhon NABIYEVA[1], Tohir AKRAMOV[2,3,4,*], Davronjon ABDUVOKHIDOV[1,2,5], Yuantao ZHANG (张远涛)[6], Maksudbek YUSUPOV[1,7] and Jamoliddin RAZZOKOV[1,8,9]

[1] Institute of Fundamental and Applied Research, National Research University TIIAME, Tashkent 100000, Uzbekistan
[2] Laboratory of Experimental Biophysics, Centre for Advanced Technologies, Tashkent 100174, Uzbekistan
[3] Department of Theoretical Physics, National University of Uzbekistan named after Mirzo Ulugbek, Tashkent 100174, Uzbekistan
[4] Institute of Nuclear Physics, Academy of Sciences of Uzbekistan, Tashkent 100214, Uzbekistan
[5] R & D Center, New Uzbekistan University, Tashkent 100007, Uzbekistan
[6] School of Electrical Engineering, Shandong University, Jinan 250061, People's Republic of China
[7] Department of Information Technologies, Tashkent International University of Education, Tashkent 100207, Uzbekistan
[8] Kokand University Andijan Branch, Andijan 170619, Uzbekistan
[9] Department of Biotechnology, Tashkent State Technical University, Tashkent 100095, Uzbekistan

[*]E-mail of corresponding author: tohir.akramov@yahoo.com

Received 16 August 2024, revised 18 December 2024
Accepted for publication 20 December 2024
Published 26 February 2025

Abstract

Cold atmospheric plasma (CAP) has emerged as a promising technology for the degradation of organic dyes, but the underlying mechanisms at the molecular level remain poorly understood. Using density-functional tight-binding (DFTB)-based quantum chemical molecular dynamics at 300 K, we have performed numerical simulations to investigate the degradation mechanism of Disperse Red 1 (DR) interacting with CAP-generated oxygen radicals. One hundred direct-dynamics trajectories were calculated for up to 100 ps simulation time, after which hydrogen-abstraction, benzene ring-opening/expanding, formaldehyde formation and modification in the chromophoric azo group which can lead to color-losing were observed. The latter was obtained with yields of around 6% at the given temperature. These findings not only enhance our understanding of CAP treatment processes but also have implications for the development of optimized purification systems for sustainable wastewater treatment. This study underscores the utility of DFTB simulations in unraveling complex chemical processes and guiding the design of advanced treatment strategies in the context of CAP technology.

Keywords: wastewater treatment, disperse red 1, cold atmospheric plasma, reactive oxygen species, reactive molecular dynamics, degradation mechanisms

(Some figures may appear in colour only in the online journal)

* Author to whom any correspondence should be addressed.

1. Introduction

The growing demand for dyes in industries such as pharmaceuticals, food, and textiles inevitably led to an increase in dye effluents discharged into wastewater [1]. These outflows pose a significant threat to aquatic ecosystems, including plants, animals, and indirectly, human beeings through the consumption of food grown in water contaminated with dyes [2–4]. Due to the intricate organic structures of dyes, conventional treatment methods such as physical, chemical, and biological approaches (including ultrasound, cavitation, UV irradiation, chlorine and ozone oxidation, and microbial treatments) are often ineffective, economically unfeasible, or may generate secondary toxic byproducts [5–8]. Consequently, researchers are exploring alternative methods to address these challenges [9–11].

One such promising approach is advanced oxidation processes (AOPs), which have attracted considerable attention worldwide [12–15]. AOP involves the generation of hydroxyl radicals (HO•) through various mechanisms. These radicals effectively break down dissolved organic compounds in wastewater, converting them into non-toxic substances. In addition to HO•, other oxidizing species such as ozone (O_3) and hydrogen peroxide (H_2O_2) also play a vital role in AOPs [16–19]. Cold atmospheric plasma (CAP) technology, a subset of AOPs, stands out among its counterparts due to its eco-friendliness, ease of production, and economic viability [20–24]. Unlike other AOPs, CAP does not necessitate costly catalysts, chemicals, or radiation [25–27]. CAP technology uses the power of ionized gas to generate reactive species capable of breaking down organic contaminants in wastewater. Unlike traditional plasma technologies, CAP operates at near-ambient temperatures, making it suitable for treating heat-sensitive materials without causing thermal damage. Additionally, CAP treatment does not require the use of chemicals or produce harmful byproducts, making it an eco-friendly option for wastewater treatment [28, 29].

Although CAP devices consume electrical power, their environmental footprint/impact is significantly reduced compared to other AOPs. The resources required for CAP primarily include the manufacturing cost of the plasma device, power supplies, and electrical energy as operational expenses.

The degradation of organic dyes using CAP has been the subject of considerable research interest with studies mainly focusing on different types of CAP devices, such as dielectric barrier discharge (DBD), plasma jet, gliding arc and corona discharge [30–33]. Rahimpour *et al* investigated the removal of crystal violet dye from a liquid using a post-discharge pulsed DBD reactor, with O_2 as the working gas [34]. In their study, oxygen was introduced into the DBD reactor, and the resulting effluent gas was bubbled through the solution. This approach enhanced the mass transfer of reactive oxygen species (ROS) into the solution, leading to a higher degradation rate of the dye. When argon was added to the working gas at a fixed input power, the dye degradation increased compared to using pure oxygen. This improvement was attributed to the formation of more ozone molecules due to the higher dissociation of oxygen molecules facilitated by argon metastables and energetic electrons in the plasma system. The degradation kinetics of crystal violet followed a first-order reaction (i.e., a type of chemical reaction where the rate at which a dye is decomposed is directly proportional to the concentration of the dye). Complete elimination of total organic carbon was achieved after the plasma treatment, indicating full mineralization (i.e., degradation into simpler inorganic substances) of the treated solution and the removal of unwanted organic carbon. Abdelmalek *et al* studied the decomposition of Orange I, Crystal Violet, and Eriochrome Black T dyes in aqueous solutions using a gliding arc discharge [35]. The plasma was generated between two diverging electrodes with the introduction of humid air. They found that the degradation of all three dyes followed first-order kinetics (i.e. the rate at which the dye concentration decreases over time is proportional to its current concentration). Additionally, they reported that the mineralization of the dyes decreased as the plasma exposure time decreased. In the study by Sun *et al* [36], a multi-needle jet with 24 needle electrodes was used to produce pulsed plasma for treating an aqueous solution containing methyl orange dye with different working gases (oxygen, air, argon, and nitrogen). A plate disc placed inside the dye solution served as the grounded electrode, and the plasma was formed in the gaseous phase between the needle electrodes and the dye solution. The decoloration rate followed the order: oxygen > air > argon > nitrogen. Additionally, it was reported that a smaller discharge gap was more effective for degradation due to the enhancement of the electric field in the gap, which leads to the formation of a large number of reactive species. Magureanu *et al* [37] investigated the removal of methylene blue from aqueous solutions using a pulsed high voltage corona discharge with multi-hollow needle electrodes arranged in a six-needle array. These needle electrodes were positioned at the bottom of the reactor, with a grounded electrode placed about 5 cm above their tips. Both electrodes were submerged in the liquid, and the discharge occurred in bubbles within the dye solution. The study examined the results of using different feed gases (air, argon, and oxygen) bubbled through the needles into the solution. The multi-needle electrodes generated a large volume of plasma, enhancing the interaction between reactive species and the dye solution. It was found that, at the same external power input, the degradation of methylene blue followed the order: oxygen > argon > air. The researchers explained that the more efficient degradation in oxygen and argon compared to air was due to the fact that in these gases more energy was used to form reactive species, whereas in air some of the energy was spent on the dissociation of nitrogen molecules. Additionally, they reported that the degradation rate of methylene blue depended on the initial dye concentration and the solution volume, with higher dye concentrations degrading more

rapidly in smaller volumes.

In recent years, significant progress has been made in understanding the mechanisms of CAP-induced degradation of organic pollutants in wastewater. Numerous studies have demonstrated the efficacy of CAP technology in treating various types of organic pollutants, including dyes, pharmaceuticals, and persistent organic pollutants [38, 39]. This has led to the development of innovative CAP reactor designs and process optimization strategies aimed at enhancing treatment efficiency and scalability. Kooshki *et al* highlighted in their study the significance of optimizing the plasma device for selective production of reactive oxygen and nitrogen species (RONS) in water to enhance both operational and economic efficiency in dye wastewater treatment [40]. They introduced a novel method for tuning RONS production. Specifically, using ceramic electrodes (Ce) and operating at higher reactor temperatures led to increased H_2O_2 production in plasma-activated water, reaching up to 16 mg/L within 30 min, while keeping nitrite production minimal. On the other hand, using copper electrodes with a water-cooling system (Cuw) resulted in higher nitrite concentrations, up to 80 mg/L within the same period, but negligible H_2O_2 production. The study also found that selective RONS production plays a crucial role in methylene blue dye degradation. The Ce setup demonstrated efficient dye degradation at a rate of 1.04 g/kWh, whereas the Cuw setup was less effective and generated additional by-products in water due to nitration mechanisms. Furthermore, a comprehensive cost estimation analysis revealed that scaling up the plasma technology could operate at lower energy costs compared to AOPs. Selective RONS production for dye degradation could lead to nearly a 30% reduction in total costs.

Central to the success of CAP treatment is the generation and utilization of ROS to initiate degradation reactions. The utilization of atomistic oxygen radicals, in particular, holds significant potential owing to their high reactivity towards organic pollutants [41, 42]. In this context, the computational investigation of specific molecular interactions becomes indispensable, allowing for a deeper understanding of reaction mechanisms [43–45].

Within this framework, density functional based tight binding (DFTB) methodology presents a powerful computational tool for simulating chemical processes with high accuracy and efficiency [46–48]. By employing DFTB, researchers can explore the energetics and dynamics of complex chemical reactions involved in CAP treatment, providing valuable insights into the degradation mechanisms of organic pollutants [49]. Xu *et al* [50] discussed the complex formation mechanisms of H_2O_2 resulting from the interaction of O atoms with water when exposed to CAPs. They noted that prior molecular dynamics (MD) simulations using reactive force fields and DFTB methods did not observe H_2O_2 formation. In their work, they employed density functional theory (DFT) in MD simulations, running 192 trajectories of a system containing $63H_2O-O$ to investigate the reaction mechanisms of O radicals in water. Their calculations revealed that triplet (ground) state oxygen was not reactive. They observed a transient oxywater-like structure, $O-OH_2$, which further evolved into perhydroxyl anion ($O-OH^-$) and its counterpart hydronium ion (H_3O^+). In most cases simulated, H_2O_2 was ultimately produced. The formation pathways of H_2O_2 were found to be highly complex for such a simple hydrogen-bonded system. They classified the mechanisms based on the sources and pathways of the H atom in the H_2O_2 molecule into: (i) H-abstraction; (ii) H-transfer ($n=3,4,5,6,7,8$); (iii) proton-delivery ($n=2,3$); (iv) proton-transfer. Their study confirmed that quantum MD simulations are more accurate for predicting the reaction mechanisms of H_2O_2 formation in such systems. Dabagh *et al* [51] conducted a study to evaluate the effectiveness of treated Carpobrotus edulis (TPCE) as a biosorbent for removing the dyes orange G (OG) and crystal violet (CV) from aqueous solutions. They characterized TPCE using FT-IR, specific surface area (S_s), point of zero charge (pHz), and SEM-EDX. The researchers tested the influence of various parameters – such as biosorbent dose, contact time, initial dye concentration, temperature, and pH – using a Taguchi experimental design with an L8 orthogonal array (five parameters at two levels). The DFTB method indicated strong binding of dyes to the adsorbent surface. Monte Carlo and MD simulations also demonstrated significant interactions between the dye and adsorbent surface.

In the study of Kandjani *et al* molecular dynamics simulations investigate reactions within a low-pressure argon-diluted methane plasma [52]. Initial molar fractions, determined by a 1D fluid model, serve as input for the simulations. Examining reaction pathways at various temperatures (300–1000 K), the study finds that higher temperatures promote the formation of diverse molecules. The progression of species such as C_2H and CH_3 reveals C_2H as a primary precursor and CH_3 as a key intermediate in forming larger molecules, clarifying pathways of plasma-induced molecule synthesis.

In this study, we focus on the degradation of Disperse Red 1 (DR1), a commonly encountered organic dye pollutant in wastewater, employing oxygen radicals (or O atoms) as reactive species. DR1 is an azo dye characterized by a structure wherein nitrobenzene is substituted at the 4-position of the phenyl group with a 4-N-ethyl-N-(2-hydroxyethyl)phenylazo group [53, 54]. It serves a dual role as both a dye and an allergen. This compound is classified as a monoazo compound and is a constituent of azobenzenes. The presence of these functional groups makes DR1 highly stable and vividly colored, but also poses challenges for its degradation. DR1 is extensively used in textile industries, poses significant environmental risks due to its persistence and potential toxicity [55, 56]. Through DFTB simulations, we aim to elucidate the intricate molecular-level interactions governing the degradation process of DR1 in the presence of O atoms generated by CAP sources.

The structure of this article is as follows. Section 2 provides information about the simulation setup, detailing the computational methodologies and parameters employed in the DFTB simulations. Subsequently, section 3 presents the simulation results and discussions, wherein we analyze the reaction pathways, energetics, and dynamics of DR1

degradation. Finally, section 4 offers concluding remarks that summarize key findings of our study, highlighting their implications for the development of advanced CAP strategies for wastewater treatment.

2. Methodology and simulation setup

2.1. DFTB approach

To gain deeper insights into the impact of ROS on the plasma-treatment process of DR1 dye and to offer atomistic-level observations of the detailed degradation mechanisms, we conducted reactive MD simulations. For this purpose, we used the DFTB method [46, 47, 57–59]. DFTB is a semi-empirical approach derived from DFT, where one considers electron interactions primarily with nearby atoms, simplifying the Hamiltonian used in calculations. DFTB employs a minimal valence-only electron basis set composed of Slater-type orbitals, which are mathematical functions used to describe the spatial distribution of electrons [57]. This minimal set is optimized for valence electrons, the outermost electrons involved in bonding. The DFT ground state electron density is denoted as ρ, the energy around a reference density ρ_0 is expanded in terms of density fluctuations $\delta\rho = \rho - \rho_0$ in the corresponding orders as

$$E[\rho] = E_0[\rho_0] + E_1[\rho_0, \delta\rho] + E_2[\rho_0, \delta\rho^2] + E_3[\rho_0, \delta\rho^3], \quad (1)$$

where ρ_0 is chosen to be the superposition of neutral atomic densities. The methods constructed in this way can contain terms up to the first, second or third order and are designated DFTB1, DFTB2 (or SCC-DFTB), DFTB3 respectively. In DFTB, the individual energy contributions are made simpler by the use of parameters. The second-order term E_2 includes the Hubbard parameter U, which reflects the chemical hardness of atoms. The third-order term E_3 requires derivatives of U. Calculating the zeroth-order term E_0 requires a minimal atomic basis set, involving two parameters per atom type.

The zeroth-order term E_0 in DFTB is found to be consistent across all three versions of the software, namely DFTB1, DFTB2 and DFTB3. Nevertheless, it is possible to achieve practical improvements in accuracy by optimizing confinement radii, which affect orbital overlaps and Hamiltonian matrix elements and, as a consequence, alter the total energy. The "MIO" parameter set was developed for DFTB2 with these optimized radii. For DFTB3, a reoptimized set, designated "3OB", was created with the objective of minimizing overbinding and providing a more accurate representation of van der Waals distances [59].

In the DFTB3 framework, Kohn-Sham molecular orbitals (Ψ_i) are expanded as a linear combination of atomic orbitals ϕ_μ: $\Psi_i = \sum_\mu c_{i,\mu}\phi_\mu$. This expansion gives an expression for the total energy which includes terms for the reference energy, repulsive interactions and higher order contributions associated with electron-electron interactions [47]:

$$\begin{aligned} E^{\mathrm{DFTB3}} &= E_0 + E_1 + E_2 + E_3 \\ &= \sum_i^{\mathrm{occ}} n_i \sum_{\mu\in a}\sum_{\nu\in b} c_\mu^i c_\nu^i H_{\mu\nu}^0 + \frac{1}{2}\sum_{a,b} V_{ab}^{\mathrm{rep}} \\ &\quad + \frac{1}{2}\sum_{a,b}\Delta q_a \Delta q_b\, \gamma_{ab} + \frac{1}{3}\sum_{a,b}\Delta q_a^2 \Delta q_b \Gamma_{ab}, \end{aligned} \quad (2)$$

The Hamiltonian matrix elements $H_{\mu\nu}^0$ are calculated using the Perdew-Burke-Ernzerhof functional and stored in Slater-Koster files for practical use. The second order interaction kernel γ_{ab} and its charge derivative $\Gamma_{ab} = \dfrac{\partial\gamma_{ab}}{\partial q_a}$ arederived to account for electron-electron interactions in thesystem. In addition, the pairwise repulsive potentials V_{ab}^{rep} are empirically fitted and tabulated as splines to facilitate efficient evaluation during simulations [59].

In the context of DFTB3, the LCAO-MO (Linear Combination of Atomic Orbitals - Molecular Orbitals) coefficients c_μ^i, c_ν^i and the Mulliken partial charges Δq_a, Δq_b are obtained by solving the secular Kohn-Sham equations:

$$\sum_\nu c_\nu^i (H_{\mu\nu} - \varepsilon_i S_{\mu\nu}) = 0 \quad \forall\mu, i, \quad (3)$$

where $S_{\mu\nu}$ is the overlap matrix representing the overlap between the atomic orbitals ϕ_μ and ϕ_ν [58].

The Mulliken charges affect the updated Hamiltonian matrix elements:

$$\begin{aligned} H_{\mu\nu} = H_{\mu\nu}^0 + S_{\mu\nu}\sum_c \Delta q_c \Bigg(&\frac{1}{2}(\gamma_{ac} + \gamma_{bc}) \\ &+ \frac{1}{3}(\Delta q_a \Gamma_{ac} + \Delta q_b \Gamma_{bc}) + \frac{\Delta q_c}{6}(\Gamma_{ca} + \Gamma_{cb}) \Bigg), \end{aligned} \quad (4)$$

and equation (3) must be solved iteratively until self-consistency is reached.

As reported in reference [49], DFTB3's computational cost is more expensive than classical reactive MD techniques like ReaxFF-MD; despite its computational complexity, DFTB3 accurately captures hydrogen binding energies and hydrogen transfer barriers without compromising speed and robustness. Additionallay, DFTB3 excels in describing resonance structures, a capability absent in ReaxFF-MD, making it a valuable tool for examining reaction process in molecular levels/scales [60].

2.2. Simulation setup

In this investigation, we applied the third-order self-consistent charge density functional tight-binding (DFTB3) method [47]. To characterize the interatomic interactions within our DFTB3-MD simulations, we utilized a parameter set known as "3OB-3-1", specifically designed for DFTB3 and applicable to organic and bio-molecules [61, 62].

As our model system, we utilized the DR1 structure, a molecule consisting of 41 atoms (molecular formula $C_{16}H_{18}N_4O_3$, MW: 314.34 g/mol) as illustrated in figure 1.

DR1 is an azo dye characterized by its chromophore

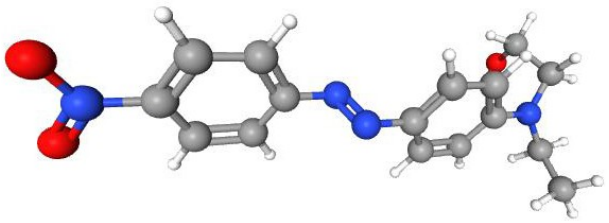

Figure 1. DR1 molecule used in our simulations. Carbon, hydrogen, nitrogen and oxygen atoms are represented by gray, white, blue and red balls, respectively.

group (−N = N−) and two benzene rings (chromogens), along with auxochromes that enhance its solubility and color properties. We considered DR1 as the target object and investigated the interaction between DR1 and atomic O, one of the reactive species produced by CAP. O radicals are favored in CAP applications due to their high reactivity, ease of production, ability to selectively produce desired reactive species, strong oxidative power, energy efficiency, and reduced risk of unwanted by-products. These advantages make them ideal for various applications, including water treatment, disinfection, and pollutant degradation. To comprehensively explore all potential bond-breaking and formation processes resulting from the impact of an O atom, and to generate some statistical insights, we conducted a substantial number of DFTB-MD simulations. Specifically, we performed 100 DFTB-MD simulations to probe the conceivable reaction mechanisms associated with the interaction of an O atom with DR1. Each simulation involved a single O atom impact, allowing us to derive statistical information on the occurring mechanisms of formed byproducts.

Note that we excluded consideration of the aqueous layer enveloping the DR1 molecule due to the high computational cost associated with the DFTB method: the inclusion of the water layer would result in excessively long calculation times [49]. Furthermore, as stated in the introduction, our investigation focused solely on the impact of an individual ROS, i.e., the O atom without consecutive impacts. This approach aimed at elucidating the influence of an individual O atom on oxidation process of pigments and assessing the closeness of simulation results to possible experimental results.

To start the simulations, the DR1 molecule was positioned at the center of a cubic box measuring 30 Å × 30 Å × 30 Å. The process of geometry optimization of the molecule was then conducted using the conjugate gradient algorithm. Subsequently, the system underwent equilibration/thermalization for 10^3 ps within an *NVT* ensemble (a system with a constant number of particles N, volume V and temperature T). The Berendsen thermostat with a coupling constant of 10^2 fs was employed during this process. The equilibration/thermalization process was realized up to the temperature $T = 300$ K when the system reached it. The number of time-steps was 2×10^6 and the Velocity Verlet method was used over integrations. A time-step of $\Delta t = 0.5$ fs was utilized in all simulations, including thermalization and subsequent particle impact simulations. Periodic boundary conditions were applied in all three spatial dimensions. A finite Fermi-Dirac electronic temperature $T_e = 1000$ K was used within DFTB. This allows for more accurate modeling of radical species and avoids incorrect ionic dissociation, making it a powerful tool for studying complex chemical reactions involving O radicals [63].

Following the equilibration, a single O atom was randomly introduced around the structure, maintaining a minimum distance of 5 Å from the molecule. It is worth to note that the box size was sufficiently large to introduce a single O atom with a random position around the molecular structure. This precautionary step (i.e., positioning the O atom at least 5 Å from the molecule) aimed to prevent initial long-distance interactions between the O atom and the DR1, particularly in terms of Coulomb and van der Waals interactions. The impact simulations constituting 100 DFTB-MD runs were conducted: each one was done for a total simulation time of $t = 100$ ps, equivalent to the number of time-steps 2×10^5. This duration was deemed sufficient for observing bond breaking and formation events within the DR1 structure. All simulations were carried out using the DFTB+ program package [59, 64].

3. Results and discussion

As indicated in the previous section, we conducted DFTB-MD simulations to explore trajectories of O atoms interacting with the DR1 molecule (see figure 1). These simulations permit to attain a more comprehensive understanding of the oxidation process and the molecular mechanisms underlying this synthetic dye degradation. Figure 2 illustrates the time

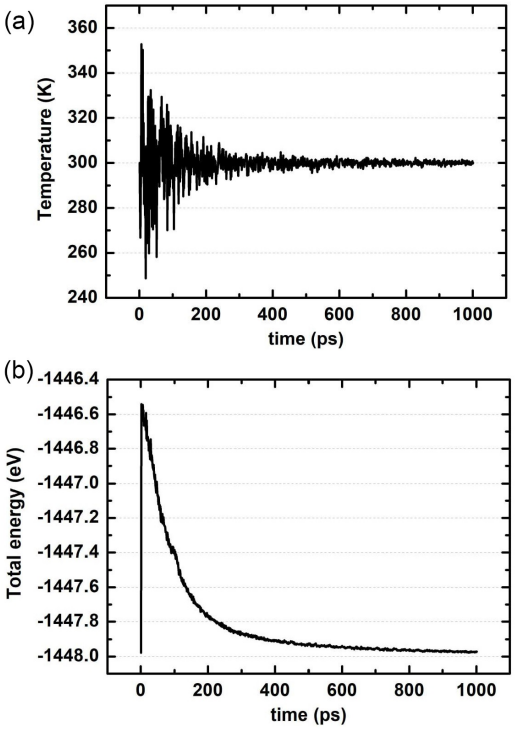

Figure 2. Time-evolutions of temperature (a) and total energy (b) during the equilibration/thermalization process over the molecular structure of DR1.

evolutions of the temperature (a) and total energy (b) of the DR1 system. As shown in the figure, a simulation time of 10^3 ps was sufficient to achieve a well-thermalized DR1 system. Thereafter, a total of 100 DFTB-MD simulations were performed and as a result, such number of different trajectories were obtained illustrating the impacts between O atom and DR1 molecule. The results are outlined in table 1 including 31 reaction mechanisms. The occurrence frequency of each reaction is given in column 4 of the table indicating how often each process was observed.

As mentioned above, DR1 possesses a chromophoric azo group (−N = N−) as a key contributor to its color, see figure 3. Additionally, the naphthalenol moiety and the surrounding aromatic structures in the molecule contribute to the overall coloration, with the extended conjugated system allowing absorption of visible light and imparting the characteristic red hue to the compound [53, 54].

3.1. Numerical results

Numerical calculations reveal that all reactions initiate with H-abstraction from a specific site on DR1, excluding those involving azo groups and ring-breaking of benzene. Put

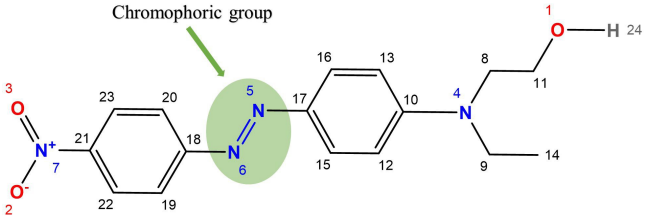

Figure 3. The molecular structure of DR 1, $C_{16}H_{18}N_4O_3$, illustrates its vibrant coloration, which stems from the presence of chromophoric groups, notably the azo group (−N = N−) and aromatic moieties. Highlighted in blue against a green background is the azo group, contributing significantly to the dye's color by absorbing visible light and imparting a distinct red hue.

Table 1. Summary of all reaction events observed in the simulations following the interaction of O atoms with the DR1 molecule (see also figure 3).

Number	Event	Frequency		Details
1	H-abstraction	C_8-OH	3	Formation of hydroxyl group
2		C_8-OH	7	
3	H-abstraction	$C_{11}-OH$	8	
4		$C_{11}-OH$	1	Formation of hydroxyl group
5		$C_{11}O_1-OH$	3	Formation of hydroperoxide group
6		C_{11} and O_1H; H_2O	3	Formation of aldehyde group
7	H-abstraction	$C_{14}-OH$	16	Formation of hydroxyl group, see figure 4
8	H-abstraction	C_9-OH	1	Formation of hydroxyl group
9		C_9-OH	1	
10	H-abstraction	$C_{12}-OH$	5	
11		$C_{13}-OH$	3	Formation of hydroxyl group
12		$C_{15}-OH$	2	
13		$C_{16}-OH$	2	
14	H-abstraction	$C_{19}-OH$	1	
15		$C_{22}-OH$	3	Formation of hydroxyl group
16		$C_{23}-OH$	1	
17	H-abstraction	H_2O and CH_2O	12	Formation of water molecule and formaldehyde (see figure 5)
18	O-addition	N_6-O	3	Addition of oxygen to the azo group (see figure 6(a)) → may lead to loss of color
19		N_5-O	3	
20	O-addition	$C_{20}-O-C_{23}$	3	Addition of oxygen to the benzene ring (see figure 6(b))
21		$C_{16}-O-C_{17}$	1	Ring-expansion
22		$C_{21}-O-C_{22}$	2	
23		$C_{10}-O-C_{13}$	1	
24		$C_{13}-O-C_{16}$	1	
25		$C_{10}-O-C_{12}$	1	
26		$C_{18}-O-C_{20}$	3	
27	O-addition	—	5	Benzene ring-opening (see figure 6(c))
28	O-addition	$C_{19}-O$	1	Addition of oxygen to C_{19}, detachment of H connected to C_{19} and binding of it to N_5, formation of ketone group
29	O-addition	N_7O_3-O	2	
30		$C_{21}=O$ and NO_2	1	Formation of $C_{21}=O$ bond, dissociation of $C_{21}-N_7$ bond and subsequent detachment of NO_2 from the system
31	O-addition	N_4+O	1	
	Total number of events		100	

differently, the oxygen atom extracts a hydrogen atom (or in certain instances, two hydrogen atoms) from the molecular structure, resulting in subsequent dissociation or formation.

The reaction mechanism most frequently observed, denoted as reaction (7) in table 1, is visually depicted in figure 4. The oxygen atom extracts a hydrogen atom from the hydroxyl group attached to C_{14} (indicated by the red arrow in figure 4), resulting in the formation of two radicals: C_{14}• and •OH Following this, these two radicals combine to form a new hydroxyl group. This category of reaction mechanism, involving H-abstraction followed by the binding of hydroxyl (OH), may also manifest in alternate sites within the DR1 molecule and emerged as the predominant reaction mechanism observed in our simulations (refer to reactions (1)–(17) in table 1). Our simulations did not anticipate the experimentally observed configuration with two or three extra oxygen atoms, as we did not investigate the consecutive impacts of oxygen atoms. However, it is plausible that oxygen addition (i.e., the generation of a new hydroxyl group) could occur subsequently at different locations within the system, potentially leading to the formation of the structures mentioned above.

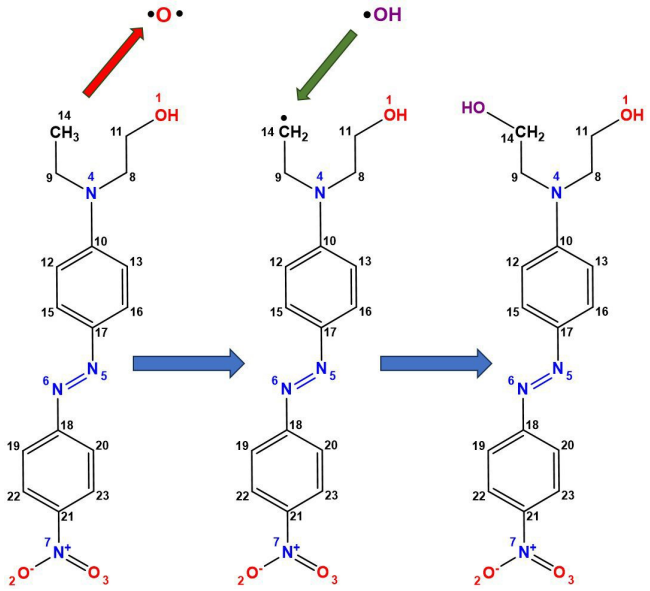

Figure 4. Visualization of the reaction mechanism wherein an O atom interacts with DR1, resulting in the generation of new OH.

Another reaction mechanisms most frequently observed, namely reaction (17) as documented in table 1, is visually represented in figure 5. The oxygen atom extracts a hydrogen atom from the alcohol group attached to C_{11} (indicated by the red arrow in figure 5), leading to the creation of two radicals: $C_{11}-O$• and •OH. This initiates a rearrangement process, disconnecting $C_{11}-O$ from the DR1 radical and resulting in the formation of a formaldehyde molecule, CH_2O. The •OH radical then takes the hydrogen bound to C_8, eventually leading to the formation of a water molecule in the system. Note that the formed DR1 radical after both the rearrangement and pulling out H bound to C_8 is not necessarily stable, that is, it can revert back, but radical molecules also notoriously rearrange, eliminate or fragment in the following steps until more stable radicals are formed. Radical molecules, notorious for their dynamic nature, are prone to undergo further rearrangements, eliminations, or fragmentations in subsequent steps, ultimately converging towards configurations of greater stability. These initial reactions, often regarded as the "first step", play a pivotal role in elucidating the onset of reaction mechanisms, which remain considerably challenging to explore through experimental observations. This kind of reaction mechanism, encompassing H-abstraction, subsequent binding of OH, and rearrangement reactions, exhibits versatility in occurrence across vari-

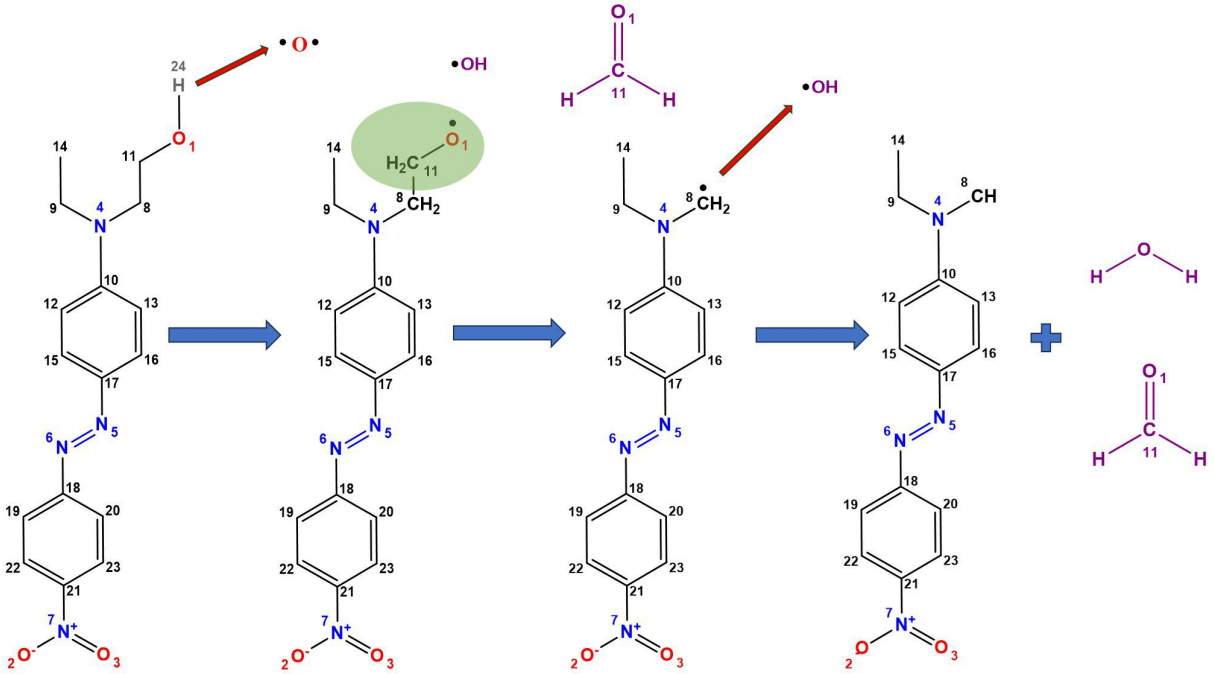

Figure 5. Visualization of the reaction mechanism wherein an O atom interacts with DR1, resulting in the generation of water and formaldehyde molecules.

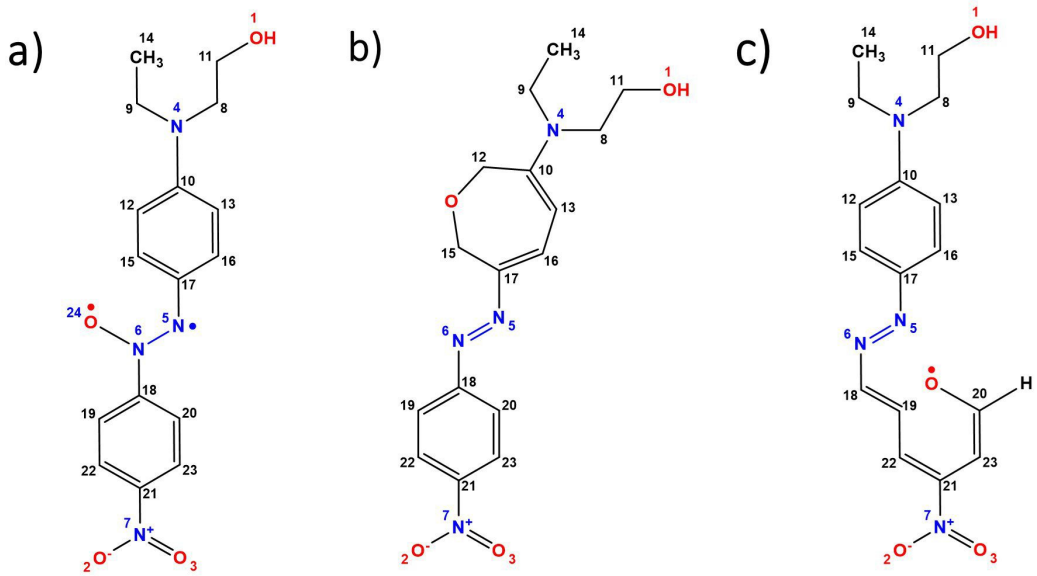

Figure 6. Visualization of three distinct reaction pathways: (a) binding of oxygen radical to the azo group, which may ultimately lead to loss of color; (b) interaction of the oxygen radical with benzene ring leading to the formation of a seven sided ring structure; and (c) ring-opening as a result of oxygen radical's interaction.

ous positions of the DR1 molecule. Notably, it emerged as second the most frequently observed reaction mechanism cases in our simulations, as evidenced by reaction (17) in table 1.

In figure 6(a), we unveiled a pivotal reaction mechanism wherein the oxygen radical intricately binds to the chromophoric groups inherent in the DR1 molecule, notably targeting the azo group. This catalytic interaction causes a profound structural shift within DR1, which subsequently has a profound influence on its color dynamics. Furthermore, in figure 6(b), the emergence of a benzene ring transformation into a heptagon, i.e. a seven-membered ring structure is visually captured, shedding light on a noteworthy structural transformation within the compound. In particular, the oxygen radical binds to two carbon atoms in the benzene ring, forming a bridge. This subsequently leads to the cleavage of the C – C bond, resulting in the formation of a seven-membered ring. Conversely, figure 6(c) illustrates a new type of phenomenon – a ring opening, hinting at the complex dynamics underlying molecular rearrangements in DR1.

Our predictive analyses extrapolate that such reactions are likely to induce a significant shift in the compound's coloration, suggesting either a complete disappearance or a noticeable alteration in its hue. This insight underscores the intricate interplay between chemical transformations and the perceptible properties of dyes. By leveraging these visual representations and predictive insights, we endeavor to unravel the complex mechanisms governing the behavior of DR1, thereby deepening our understanding of its chemical intricacies and broadening its potential applications across diverse scientific domains. In addition to the observed reactions, we have identified several other noteworthy reactions. These include instances where oxygen radicals interact with nitrogen atoms at positions N_7 and N_4 (see reactions (29) and (31) in table 1, respectively), leading to chemical modifications within the molecule. Furthermore, oxygen radicals bind with C_{21}, resulting in the formation of NO_2 and subsequent detachment of it from C_{21}. Additionally, another reaction (i.e., reaction (28) in table 1) involves the combination of oxygen radicals with C_{19}, leading to the transfer of a hydrogen atom from C_{19} to N_5. These reactions contribute to the complex array of transformations occurring within the molecular structure.

3.2. Discussion

The degradation of DR1 dye using the CAP mechanisms leverages the reactivity of O• radicals generated during the plasma process. These radicals initiate various reactions that break down the dye's complex molecular structure. This includes:

- Attack on azo group (–N = N–): O• radicals are highly reactive and target the azo group, most likely cleaving the nitrogen-nitrogen double bond, which was not observed during the simulation time used in our study (i.e., 100 ps). It should be mentioned that in our DFTB-MD simulations, we applied non-consecutive (discontinuous) impacts of oxygen radicals, where each MD run begins with an intact dye molecule. We refer to this approach as simulating a low plasma dosage. As a result, under these conditions, we did not observe any cleavage of the N = N double bond, indicating that the low plasma dosage is insufficient to break the N = N bond responsible for the dye's color. To determine whether consecutive impacts (where an oxygen atom interacts with a dye molecule already modified in a previous MD run) – representing a high plasma dosage – would affect N = N bond cleavage, we conducted test simulations. These test runs (not shown here) did result in N = N bond cleavage, effectively accelerating molecular degradation. Thus, a high plasma dosage is necessary to cleave the N = N bond, which leads to dye

decolorization and eventually results in its degradation.

- Interaction with chromogens (benzene rings): following the cleavage of the azo bond, O• radicals can attack the benzene rings. This leads to the formation of smaller, less complex molecules. The oxidative cleavage of these aromatic rings is essential for complete mineralization of the dye.

Auxochromes in DR1, such as hydroxyl (−OH) and amino ($-NH_2$) groups, influence the dye's reactivity. They can enhance the dye's interaction with reactive species, facilitating the breakdown of the molecular structure. The interactions between O• radicals and auxochromes can lead to the formation of intermediate compounds, which further degrade into harmless end products like H_2O and CO_2.

During the degradation process, various intermediates are formed:

- Perhydroxyl anion ($O-OH^-$): this intermediate is formed during the initial stages of oxidation and can participate in further reactions leading to the formation of HO• radicals.
- Hydronium ion (H_3O^+): this ion forms alongside perhydroxyl anion and contributes to the acidic environment that can enhance further degradation reactions.
- Hydroxyl radicals (HO•): these radicals are highly reactive and play a significant role in breaking down the remaining molecular fragments, leading to complete mineralization.

Our results can be contextualised with those of reference [56], where da Silva Leite *et al* evaluated the ecotoxicity and degradation pathways of the azo dye DR1 using the photo-Fenton process. Their analysis, using HPLC-DAD and LC-MS/MS, showed that early stages of degradation increased toxicity due to intermediates, while prolonged treatment eventually reduced toxicity. The study identified most of the intermediates as products of hydroxyl radical addition to the aromatic ring, with some azo bond cleavage. In contrast, our study modelling CAP-induced degradation suggests a different degradation pathway. We observed that the degradation of DR1 under CAP treatment is faster and involves reactive oxygen species. Interestingly, we also identified intermediates that retain the azo group, which is partially consistent with photo-Fenton results. However, the development of toxicity under CAP treatment appears to be different. While da Silva Leite *et al* emphasised the adjustment of reaction time to control toxicity, our computational results suggest that optimizing the intensity and duration of CAP treatment could similarly minimise toxic by-products. Toxicity monitoring is therefore essential for both treatments to ensure environmentally safe degradation.

4. Conclusions

This study offers comprehensive insights into the interaction mechanisms of Disperse Red 1 (DR1) with oxygen radicals (a key ROS component) generated by cold atmospheric plasma (CAP), employing reactive DFTB-MD simulations. The research revealed that the primary initiation step involves hydrogen abstraction by oxygen radicals, a mechanism that plays a crucial role in facilitating subsequent dissociation and molecular rearrangements. Notably, the most common reactions involved hydrogen abstraction from various locations on the DR1 molecule, resulting in the formation of new hydroxyl groups and other reactive intermediates. Additionally, a significant secondary mechanism included hydrogen abstraction, leading to the formation of formaldehyde and water, which underscored the complexity of radical-driven rearrangement processes.

Importantly, the study also highlighted key interactions between oxygen radicals and the chromophoric azo group, as well as transformations of benzene rings, resulting in the formation of seven-membered rings or ring openings. These structural changes are predicted to alter or eliminate the color of the compound, reflecting the profound impact of CAP treatment on DR1's chemical properties.

While the simulations focused on low plasma dosages, which did not show cleavage of the N = N double bond, test simulations indicated that high plasma dosages can break this bond, accelerating decolorization and complete dye degradation. This finding emphasizes the importance of optimizing CAP treatment intensity to achieve effective pollutant breakdown while minimizing toxic by-products.

Our computational results were compared with experimental findings. While both approaches revealed the formation of intermediate products, our study demonstrated that CAP treatment can result in faster degradation with distinct intermediate profiles. This comparison underscores the potential for tailored CAP strategies to efficiently degrade complex dye structures, guiding future research and experimental validation for safe and sustainable wastewater treatment.

Overall, this work advances our understanding of DR1 degradation under CAP, paving the way for further integration of computational and experimental approaches to refine treatment processes, optimize plasma parameters, and address emerging environmental concerns.

Author contributions

Namunakhon NABIYEVA, Tohir AKRAMOV and Davronjon ABDUVOKHIDOV analyzed the data. Tohir AKRAMOV and Davronjon ABDUVOKHIDOV drafted the manuscript, while Yuantao ZHANG, Maksudbek YUSUPOV and Jamoliddin RAZZOKOV provided critical revisions. Maksudbek YUSUPOV contributed to the preparation of the model system and conducted the MD simulations. Jamoliddin RAZZOKOV supervised the work.

Acknowledgments

The authors gratefully acknowledge the financial support from the Ministry of Higher Education, Science, and Innova-

tions of the Republic of Uzbekistan (Nos. AL-4821012320 and AL-5921122141).

References

[1] Sathya K *et al* 2022 *Appl. Water Sci.* **12** 70
[2] Clark M 2011 Handbook of textile and industrial dyeing: principles, processes and types of dyes (Cambridge: Woodhead Publishing)
[3] Bashir I *et al* 2020 Concerns and Threats of Contamination on Aquatic Ecosystems In: Hakeem K R, Bhat R A and Qadri H *Bioremediation and Biotechnology: Sustainable Approaches to Pollution Degradation* Cham: Springer 2020: 1 doi: 10.1007/978-3-030-35691-0_1
[4] Daniel Enns *et al* 2023 *Water Res.* **243** 120388
[5] Ahmed M *et al* 2022 *npj Clean Water* **5** 12
[6] Manish Kumar *et al* 2023 *Environ. Pollut.* **320** 121009
[7] Fakhri B *et al* 2024 *Sustain. Environ.* **10** 2322831
[8] Zhou S *et al* 2024 *Water Sci. Tech.* **89** 1539
[9] Alsukaibi A K D 2022 *Processes* **10** 1968
[10] Donkadokula N Y, Kola A K and Saroj D 2020 *Sustain. Environ. Res.* **30** 9
[11] Kesari K K *et al* 2021 *Water Air Soil Pollut.* **232** 208
[12] Garrido-Cardenas J A *et al* 2019 *Int. J. Environ. Res. Public Health.* **25** 17
[13] Lucas M S, Peres J A and Li Puma G 2021 *Water* **13** 1309
[14] Chen Y D *et al* 2021 *Chem. Eng. J.* **409** 128207
[15] Saravanan A *et al* 2022 *Chemosphere* **308** 136524
[16] Litter M I and Quici N 2010 *Recent Patents Eng.* **4** 217
[17] El-Gawad H A *et al* 2023 *Sci. Rep.* **13** 3420
[18] Arifin M N *et al* 2023 *Environ. Res.* **229** 115936
[19] Suwannarat S *et al* 2024 *ACS Appl. Bio. Mater.* **7** 1469
[20] Adamovich I *et al* 2017 *J. Phys. D: Appl. Phys.* **50** 323001
[21] Nishijima A *et al* 2019 *Mod. Plast. Surg.* **9** 18
[22] Domonkos M *et al* 2021 *Appl. Sci.* **11** 4809
[23] Christos A 2022 *Chem. Eng. J.* **428** 131657
[24] Cyganowski P *et al* 2023 *Plasma Chem. Plasma Process.* **43** 199
[25] Locke B R *et al* 2006 *Ind. Eng. Chem. Res.* **45** 882
[26] Motyka A *et al* 2018 *Biotechnology and Bioengineering.* **115** 1581
[27] Upadrasta A *et al* 2023 *Journal of Applied Microbiology.* **134** lxad181
[28] Malik M A 2010 *Plasma Chem. Plasma Process.* **30** 21
[29] Morin-Crini N *et al* 2022 *Environ. Chem. Lett.* **20** 1333
[30] Tao X M *et al* 2016 *J. Environ. Manage.* **184** 480
[31] Kumar A *et al* 2021 *Eur. Phys. J. D* **75** 283
[32] Takeuchi N and Yasuoka K 2020 *Jpn. J. Appl. Phys.* **60** SA0801
[33] Yin Y *et al* 2023 *Appli. Sci.* **13** 12631
[34] Rahimpour M *et al* 2019 *J. Environ. Chem. Eng.* **7** 103220
[35] Abdelmalek F *et al* 2006 *Ind. Eng. Chem. Res.* **45** 23
[36] Sun B *et al* 2012 *J. Environ. Sci.* **24** 840
[37] Magureanu M *et al* 2008 *Plasma Chem. Plasma Process.* **28** 677
[38] Zeghioud H *et al* 2020 *J. Water Process Eng.* **38** 101664
[39] Laroussi Mounir *et al* 2022 *IEEE Trans. Radiat. Plasma Med. Sci.* **6** 127
[40] Kooshki S *et al* 2024 *J. Water Process Eng.* **63** 105477
[41] Hefny M M *et al* 2016 *J. Phy. D: Appl. Phy.* **49** 404002
[42] Benedikt J *et al* 2018 *Phys. Chem. Chem. Phy.* **20** 12037
[43] Lin P 2020 *J. Phy. D: Appl. Phy.* **54** 075205
[44] Zhang Y T, Gao S H and Ai F 2023 *Front. Physics.* **11** 1125548
[45] Elaissi S and Alsaif N A M 2023 *Polymers* **15** 1235
[46] Elstner M *et al* 1998 *Phys. Rev. B* **58** 7260
[47] Gaus M, Goez A and Elstner M 2013 *J. Chem. Theory and Comput.* **9** 338
[48] Elstner M, Frauenheim T and Sándor S 2003 *J. Mol. Struct.: THEOCHEM.* **632** 29
[49] Yusupov M *et al* 2023 *Plasma Processes Polym.* **20** 2200137
[50] Xu S F, Jirasek V and Lukes P 2020 *J. Phys. D: Appl. Phys.* **53** 275204
[51] Dabagh A *et al* 2023 *Heliyon* **9** e21977
[52] Kandjani G O *et al* 2023 *Plasma Process. Polym.* **20** e2200192
[53] del Pilar Carreón-Castro, M. *et al* 2010 *Thin solid films* **518** 4136
[54] Guo X Y *et al* 2021 *Chin. J. Org. Chem.* **41** 1703
[55] Fernandes F H, Bustos-Obregon E and Salvadori D M F 2015 *Reprod Toxicol.* **53** 75
[56] da Silva Leite L *et al* 2016 *Chemosphere* **148** 511
[57] Porezag D *et al* 1995 *Phys. Rev. B.* **51** 12947
[58] Seifert G, Porezag D, and Frauenheim T 1996 *Int. J. Quantum Chem.* **58** 185
[59] Hourahine B *et al* 2020 *J. Chem. Phys.* **31** 152
[60] Qian H J *et al* 2011 *J. Chem. Theory Comput.* **7** 2040
[61] Gaus M *et al* 2014 *J. Chem. Theory Comput.* **10** 1518
[62] Kubillus M *et al* 2015 *J. Chem. Theory Comput.* **11** 332
[63] Saha B *et al* 2009 *ACS Nano.* **3** 2241
[64] Aradi B, Hourahine B and Frauenheim T 2007 *J. Phys. Chem. A* **111** 5678